Circulation Patterns Associated with Current and Future Rainfall over Ethiopia and South Sudan from a Convection-Permitting Model

Herbert O. Misiani [1],*, Declan L. Finney [2], Zewdu T. Segele [1], John H. Marsham [2], Abebe Tadege [1], Guleid Artan [1] and Zachary Atheru [1]

[1] IGAD Climate Prediction and Applications Centre (ICPAC), Nairobi 10304-00100, Kenya; zsegele@icpac.net (Z.T.S.); atadege@icpac.net (A.T.); gartan@icpac.net (G.A.); zatheru@icpac.net (Z.A.)

[2] Faculty of Environment, University of Leeds, Leeds LS2 9JT, UK; D.L.Finney@leeds.ac.uk (D.L.F.); J.Marsham@leeds.ac.uk (J.H.M.)

* Correspondence: misianihabat@icpac.net

Abstract: Ethiopia and South Sudan contain several population centers and important ecosystems that depend on July–August rainfall. Here we use two models to understand current and future rainfall: the first ever pan-African numerical model of climate change with explicit convection and a parameterized model that resembles a typical regional climate model at 4.5 and 25 km horizontal grid-spacing, respectively. The explicit convection and higher resolution of the first model offer a greatly improved representation of both the frequency and intensity of rainfall, when compared to the parametrized convection model. Furthermore, only this model has success in capturing the east–west propagation of rainfall over the full diurnal cycle. Enhanced low-level westerlies were found for extremely wet days, though this response was weaker in the explicit convection model. The increased orographic detail in the explicit model resulted in the splitting of the low-level Turkana Jet core into smaller cores, and inhibited its penetration far into South Sudan. Some projected changes were found to be independent of model, such as changes in the strength of Somali and Turkana jets, as well as the shifting of Turkana jet core to lower levels. However, the explicit model end-of-century projections showed a larger and clearer decrease in wet days, accompanied by an increase in wet day intensity and extreme rainfall. This study highlights serious limitations of relying solely on simulations which parameterize convection to inform decisions in the region of South Sudan and Ethiopia.

Keywords: convection-permitting; climate change; Ethiopia; South Sudan; rainfall; Turkana jet

1. Introduction

The Greater Horn of Africa is a region characterized by frequent extremes that have over the years caused great loss of life and impacted negatively on the economy of the region. Both the sudden and slow-onset extremes in addition to other triggers and drivers have often contributed to large scale displacements and conflicts in many parts of the region [1]. Ethiopia and South Sudan are two examples of countries, within the northern parts of the region, which have continually been impacted by climate extremes. Ethiopia is one of Africa's fast-growing economies and the second most populous country in Africa while South Sudan is the youngest country in Africa and has been under conflicts since its separation from the north. Both countries are dependent on rainfall for key sectors such as agriculture and energy. Apart from the likelihood of the key sectors being impacted by future extreme climate events, additional challenges such as conflicts, diseases, and migration may be further exacerbated under increased global warming. Some key features, such as the Sudd wetlands, national parks,

as well as the White and Blue Nile rivers, found within the two countries could be under threat from both human and climate factors [2,3]. These features are important for microclimates in the region, support the ecosystem and livelihoods of people within these two countries including neighboring countries especially Sudan and Egypt [2,3]. Therefore, rainfall characteristics in some of these areas are critical not only to these two countries but also to countries further downstream of the major rivers.

Although there exist areas within South Sudan and Ethiopia that receive rainfall patterns similar to the equatorial East Africa (i.e., rain during March–May and October–December), most regions within these two countries experience one dominant rainy season in Boreal summer, known locally as the Kiremt in Ethiopia [4]. This season is important for the cropping regions, accounting for more than 50% of annual rainfall [5]. The atmospheric dynamics involved in rain generation over the two countries are more related to the West African and Indian monsoons [6,7]. The location and orography of Ethiopia and South Sudan generate unique interactions between the south-easterly low-level Turkana jet that flows from Kenya and Somalia year-round [8,9], with middle and upper-level easterly jets, and with mesoscale flows generated by the Ethiopian highlands [4,10] and moisture from the Gulf of Guinea, the Indian Ocean, the Congo basin, the Mediterranean, and the Red Sea [6,11–13].

The progression of rainfall onset in Ethiopia is from the south-west (early-to-mid March) to north-east (mid-to-late July) while cessation is in the reverse direction [4]. Onset of rainfall is usually associated with the presence of shallow westerlies and a weakening of the Somali Low-Level Jet while the cessation of rainfall is usually associated with the strengthening of the Somali Jet which enhances wind divergence and wind shear over the north eastern parts of the GHA [4,14]. The shallow lower tropospheric westerlies, also known as the West Africa monsoon, persist almost throughout the season and they are predominantly overlain by easterlies aloft [4,7].

Other factors that contribute to the variability of June–September (JJAS) rainfall include Quasi-Biennial Oscillation (QBO), Southern Oscillation Index (SOI), Tropical Easterly Jet (TEJ) over the Arabian Sea, Mascarene and St. Hellena high pressure cells, El Niño-Southern Oscillation (ENSO), and the Indian Ocean Dipole (IOD) mode [10,15–17]. Additionally, wet conditions during JJAS season are associated with changes in the zonal and meridional integrated moisture fluxes, and the gradient of vertical moist static energy [17].

It is clear that future changes in rainfall driven by climate change during this key season could impact not only these two countries but other countries as well. Adaptation and mitigation measures based on robust climate information should be in place to prepare for any negative impacts in the future. Quite a number of climate change studies have been done focusing on the East Africa and the Greater Horn of Africa regions [18–22]. However, a shortcoming of the previous studies is that they use parametrized convection. In addition, the coarse models used do not successfully represent the complex orography reducing confidence in their ability to capture details of the local circulation systems such as small-scale processes critical for influencing Turkana Low Level Jet (TLLJ) variability [23].

Already, the use of high-resolution reanalysis datasets has yielded new insights into the structure and variability of the TLLJ as well as its association with boreal summer rainfall [23]. These studies have further increased our knowledge of TLLJ from previous studies that utilized coarse resolution reanalysis data and relatively short length of observations [7,24,25]. Vizy and Cook [23] found that the most important influence of TLLJ on boreal summer rainfall is on low-level convergence and shifting of zonal moisture gradient. Further, the TLLJ strength was found to influence the frequency of heavy rainfall events as well as their timing to the west of the jet exit region. Additionally, it has been shown that the TLLJ strength is negatively correlated with precipitation over eastern South Sudan and Ethiopian highlands [23].

Noting the added value in using high resolution data in this region, we utilized the first decade-long, convection-permitting climate change simulations for the Africa domain to investigate the relationship between circulation systems and extreme rainfall in the region, as well as provide the first focus on the region with this state-of-the-art dataset. Additionally, these datasets present an unprecedented opportunity to investigate the potential effects of climate change on the regions of South Sudan and Ethiopia.

Convection-permitting models explicitly simulate organized propagating storms [26] and allow vertical shear in horizontal winds to directly affect storm organization, which may be important for climate change [27]. Added value in convection permitting simulations has been found in, among other things, the simulation of the vertical structure of clouds, coupling between moist convection and convergence, the water budget, and in the continental-scale flow [28–32]. For East Africa, permitting explicit convection has recently been shown to improve some model bias in seasonality, and affect projected changes in seasonality under climate change [33]. Although convection-permitting models still have challenges in representing small-scale convective features and convection over the ocean [34], they have been shown to greatly improve representation of larger storms when compared to parametrized convection models [26] and they have often been shown to give larger climate changes in extreme rainfall. This has recently been demonstrated for Africa [35–39] and so these high-resolution models are invaluable tools for understanding the characteristics of the current African climate and how this may change under global warming. Kendon et al. [40] took a pan Africa perspective, and Finney et al. [37] focused on the bimodal rainfall region of East Africa, whilst here we focus on Ethiopia and South Sudan, in the boreal summer, where moisture is supplied by the westerly West Africa Monsoon (WAM) winds, but with additional influences from easterlies from the Indian Ocean.

2. Data and Methods

2.1. Model Simulations

A set of two model runs from the Met Office Unified Model with the same domains covering the entire African continent were used in the study [34]. One simulation allows convection to develop explicitly at a fairly uniform horizontal grid spacing of ≈4.5 km (CP4) while the other parameterizes convection at horizontal grid spacing of ≈25 km (P25). The vertical resolution of the CP4 model is 80 levels with the maximum level at 38.5 km above ground level (AGL) and was configured with higher resolution in the boundary layer and troposphere [34]. The vertical resolution of P25 is 63 levels and its maximum level is at 41 km AGL [34]. At 4.5 km grid-spacing, convection is partially resolved: much of the key dynamics of large organized systems of deep convection will be resolved, but smaller scales, such as individual cumulonimbus updraughts or entrainment is not well resolved, but are nevertheless explicitly modeled. For current climate, both models are forced by sea surface temperature (SST) analysis product by [41], available at a horizontal grid spacing of 0.25°- and 1-day temporal resolution, after bilinear interpolation onto the regional model grids [34]. Future simulations are forced by adding ΔT to the current-climate observations-based SSTs calculated at each grid cell and at monthly timescale as the climatological decadal mean change in SST between the end of century and the present-day Hadley Centre Global Environment version 2 Earth System (HadGEM2-ES) global climate model simulations [37]. The lateral boundary conditions in both models were provided by the N512L85 global atmospheric model using the Global Atmosphere/Land 7.0 120 (GA7/GL7) configuration driven by the same SST dataset [34,35]. For an in-depth description of the model configuration please refer to [31,34,37].

The current-climate simulation period is January 1997–February 2007 with the first two months representing the spin up period. Future model runs were for a representative decade around ≈2100 [36] based on the RCP8.5 scenario [42]. Both models have similar model physics except that convection is parameterized within the P25 model and it uses a different cloud and boundary layer scheme [36]. It should be noted that these models were not fine-tuned for the African climate [34]. For detailed description of model configurations, see [35,36]. The temporal resolution of the data used in this study is 1-hourly and 3-hourly for rainfall and wind, respectively. Analysis was done at seasonal, daily, and subdaily time scales after regridding to P25 resolution. Whilst differences between the models in the parametrization of convection will be a major cause of differences between the simulations, there will also be effects due to differences in model physics and cloud schemes. Such effects cannot be quantified with this dataset; however, the majority of results discussed in this study are consistent with

past convection-permitting studies of different regions, and current understandings of problems with existing parameterizations of moist convection [28,43], and therefore can more reliably be attributed to the use of explicit convection. A further source of uncertainty arises from the use of a single simulation for each model; a different driving global model would give a different evolution of global climate. However, we manage this uncertainty source by focusing on results where there are significant differences between CP4 and P25, and which are supported by arguments of the physical mechanisms, and are, therefore, likely to be applicable to any model with parameterized convection. The CP4 dataset generated under the Future Climate For Africa (FCFA) Improving Model Processes for African Climate (IMPALA) project is publicly available, with currently a limited set of hourly and monthly mean variables downloadable from the Centre for Environmental Data Analysis (CEDA) archive (http://archive.ceda.ac.uk/ and search for CP4).

### 2.2. Satellite Rainfall Estimates

The historical simulations were validated using Climate Prediction Center (CPC) MORPHing technique (CMORPH) and Tropical Rainfall Measuring Mission (TRMM) Multisatellite Precipitation Analysis 3B42 (hereafter referred to as TRMM) rainfall estimates. The CMORPH rainfall estimates are derived from passive microwave observations and then precipitation features are transported by spatial propagation information obtained from geostationary satellite IR data at 0.0727° ($\approx$8 km) horizontal grid resolution [44]. TRMM uses a calibration-based sequential scheme to combine satellite rainfall estimates from multiple satellites which is then bias corrected using monthly rain gauge data [45]. TRMM datasets are available in both lagged and near-real time from 1998 to present at 0.25° horizontal grid spacing. The main difference between these two products is that in CMORPH, the passive microwave-based rainfall estimates are propagated using motion vectors from infrared data derived from geostationary satellites [44]. The satellite rainfall estimates were also regridded to the P25 model's grid.

Studies that have assessed the performance of most satellite rainfall estimates concur that they perform relatively well although this depends on how and over which area the data is assessed. For example, aggregation of hourly data to daily or monthly tend to reduce the random errors hence assessments at monthly or seasonal time scales may result in reduced random errors [46]. Dinku et al. [47] found that TRMM, CMORPH, and other satellite rainfall products suffered from high random errors and performed poorly in simulating grid scale rainfall amount. In particular, CMORPH overestimates rainfall at low elevations but does relatively well at high elevations [48]. Both TRMM and CMORPH have shown similar results in terms of bias, spatial structure, elevation dependence, and distribution functions [49]. These datasets are recommended for validating models at subdaily time scales and monitoring extreme events [45].

2.3. Subregions Used in Analysis

Three subregions were defined to aid in the determination of the patterns of circulation during extreme rainfall events. Figure 1 shows the three boxes used superimposed on topography of the region. The digital elevation model is from the Global Land One-Kilometer Base Elevation (GLOBE) available at the National Oceanic and Atmospheric Administration, National Geophysical Data Center [34,50]. The boxes were chosen based on spatial patterns of different rainfall indices (such as wet day frequency, mean rainfall, and extreme rainfall) using subjective and objective (Empirical Orthogonal Function Analysis) approaches. Additionally, the boxes were chosen based on the significance of rainfall in a particular region during the season considered and the social as well as economic importance of the region. For example, Box A (Western Ethiopia box) was intentionally placed over the Ethiopian highlands due to the significance of rainfall in this region during the June–September (JJAS) season. Moreover, there are key infrastructural projects within this region that will depend on rainfall variability such as the Grand Ethiopian Renaissance Dam on the Blue Nile. Boxes B and C (Turkana Outflow and Western South Sudan boxes, respectively) were chosen because of the potential influence of the Turkana

Jet on storms propagating westwards from Western Ethiopia (Box B) and due to the significance of national parks and nature reserves (Box C). Additionally, we defined two transects based on [8]; one which is perpendicular and the other parallel to the Turkana jet axis, represented by blue and red lines, respectively, in Figure 1, to aid with the in-depth analysis of the Turkana jet.
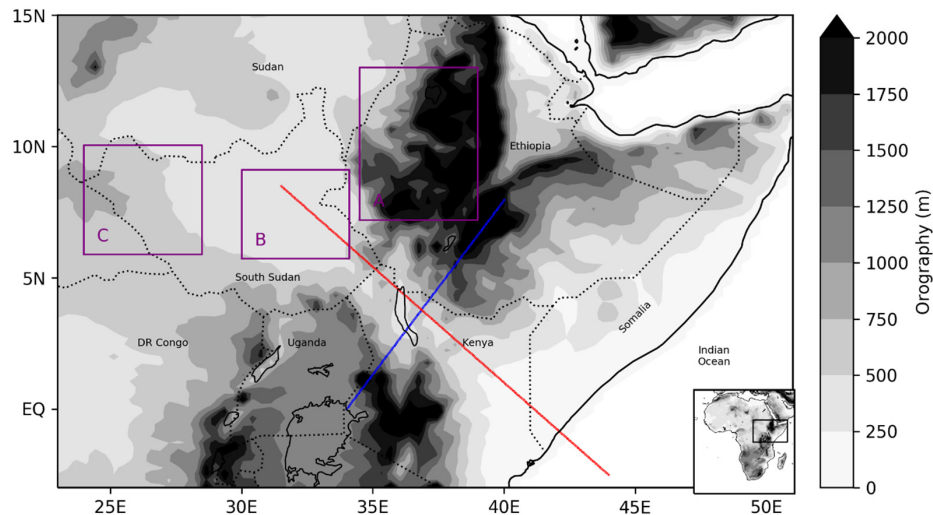
Figure 1. Area of study showing the orography and boxes/regions of interest and transects of the Turkana jet. Boxes A, B, and C correspond to Western Ethiopia, Turkana Outflow, and Western South Sudan Boxes, respectively, as defined in [8]. Blue and red lines represent transects perpendicular and parallel to the Turkana jet axis, respectively. The bottom-right inset shows the full CP4A model domain over Africa. The digital elevation model is from the Global Land One-Kilometer Base Elevation (GLOBE) dataset [50]. The equivalent plot using P25 orography is shown in the supplementary material, Figure S1.

2.4. Season for Analysis

March–May and October–December seasons have been extensively covered within the Integrating Hydro-Climate Science into Policy Decisions for Climate-Resilient Infrastructure and Livelihoods (HyCRISTAL) project's climate studies [31,37]. Initially, our main season of interest was the northern hemisphere boreal summer (June–September) rainfall season when much of South Sudan and Ethiopia receive significant rainfall [4]. However, after assessing rainfall metrics and wind fields at different levels, we found that the spatial patterns of rainfall were most coherent during July and August, which are also the peak rainfall months. Therefore, June and September were considered as transition months which might be having additional drivers to those of July and August. The analyses presented are therefore of July and August.

## 3. Results

3.1. Climatology of Rainfall and Dynamics

The rainfall and dynamics of the P25 and CP4 models were evaluated using a series of indices. The term "climatology" is used here to refer to a 9-year mean in both rainfall and wind fields. Figure 2 shows results for rainfall evaluation with reference to CMORPH and TRMM based on rainfall total, mean rainfall intensity on wet days (hereafter referred to as "wet day intensity" and calculated by taking the mean of days with rainfall > 1 mm/day), and frequency of wet days. CMORPH and TRMM show that, during July and August, a substantial amount of rainfall falls over the Ethiopian highlands. Meanwhile, there is little rainfall over northern Kenya, southeast Ethiopia to the border with Somalia at this time of year. South Sudan also experiences substantial rainfall at this time of year, its peak rainfall season. The differences between regions manifest most strongly as differences in the frequency of rainfall days compared to the differences in the other rainfall indices. The mean daily rainfall intensity ranges from 5 to 15 mm/day in most locations for which July–August is the main rainy season.
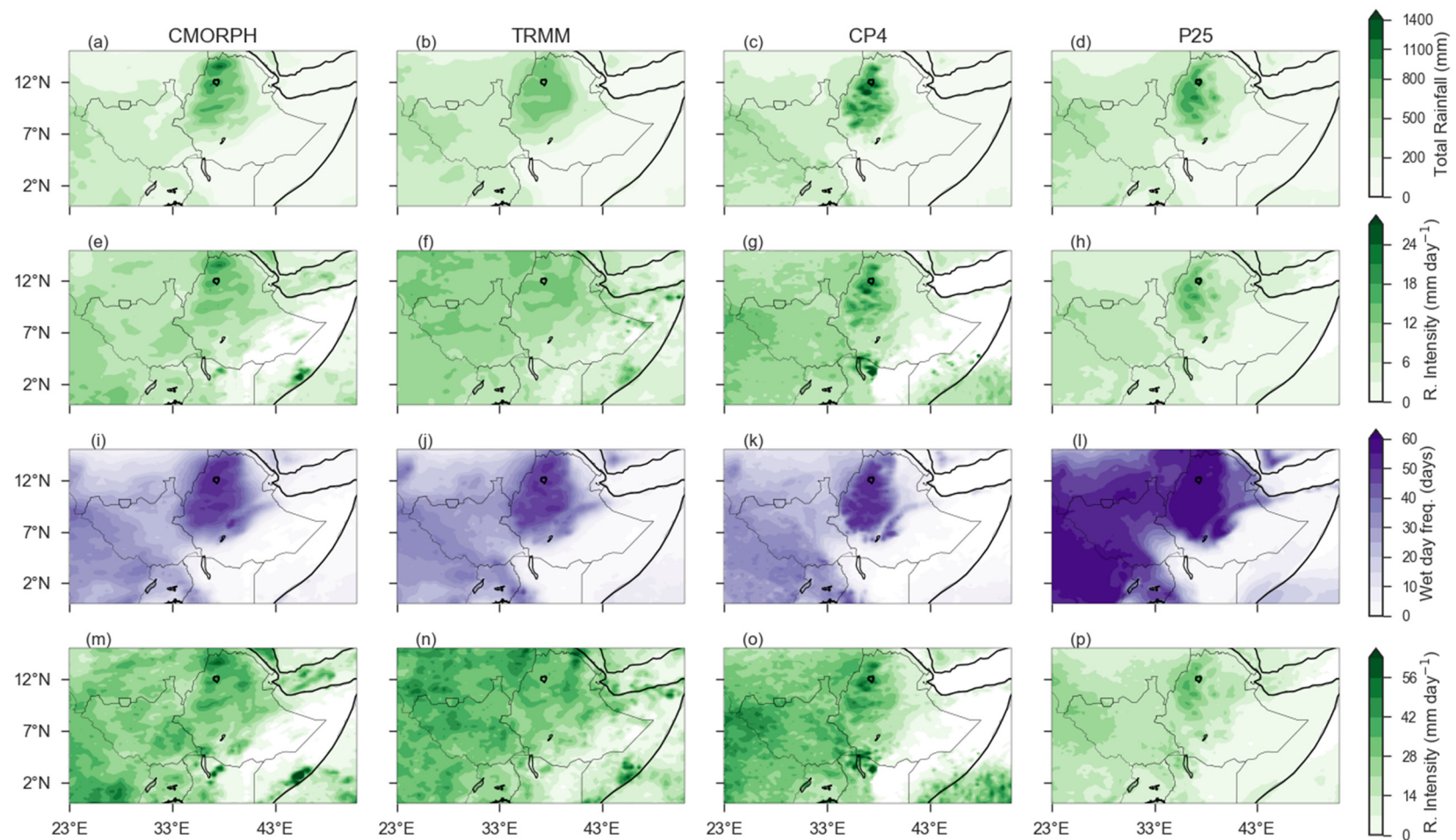
Figure 2. Evaluation of CP4 and P25 models based on different indices with a focus on the July–August season for the 1998–2006 climatological period. The rows represent total rainfall (**a–d**), mean wet day intensity (**e–h**), mean frequency of wet days (**i–l**), and the mean 95th percentile of rainfall (**m–p**), respectively, while columns represent data sources.

Both the CP4 and P25 models broadly capture the spatial patterns of the three metrics. The CP4 model simulates a higher spatial maximum of wet-day intensity than both CMOPRH and TRMM over the Ethiopian highlands. However, satellite observations show large biases in this region [51] and therefore it is difficult to accurately evaluate rainfall of models over the highlands. The wet-day intensity of P25 is lower than CP4 and in many places less than the observational estimates. On the other hand, P25 shows much higher frequency of rainfall than CP4 and the satellite estimates. This kind of bias is typical of parametrized convection models [52]. Similarly, as expected from studies of biases in parameterized convection models, the simulation of extreme rainfall by the P25 model is too low and this is much better represented by CP4 [36,37,52]. The results here therefore provide evidence that rainfall intensity and frequency in this important rainfall season for Ethiopia and South Sudan is better simulated by the explicit convection simulation than the parametrized convection simulation. This therefore provides a strong alternative perspective to traditional regional climate models when projected future changes in these rainfall metrics.

Interactions of winds in this region with the mountains are key to generating the spatial differences in rainfall just shown in Figure 2 [7]. The 500 and 200 hPa levels in CP4 and P25 show that there are strong easterly to north easterly mid and upper levels winds (Figure 3a,b,d,e). These are associated with the African Easterly Jet (AEJ) and the Tropospheric Easterly Jet (TEJ) [4,53], respectively. At 850 hPa, we see low-level south-westerlies across South Sudan towards the Ethiopian highlands flowing from the Congo. These winds are associated with humid air from the Congo basin and eastern Atlantic [4,23]. Strong winds occur in the Turkana channel flowing northwest towards South Sudan from Kenya and Somalia; this is the Turkana Jet, with its moisture more likely to originate from the Indian Ocean [23–25]. Finally, a broad low-level jet, known as the Somali Jet [54], flows at 850 hPa from the Indian Ocean onto the African continent before curving towards the northeast, over and along the coast of Somalia. The P25 model shows similar results to those of the CP4 model. The presence of all these well-known features in both models is promising, and allows us to look more closely at impacts of the two model configurations and their relation to rainfall.
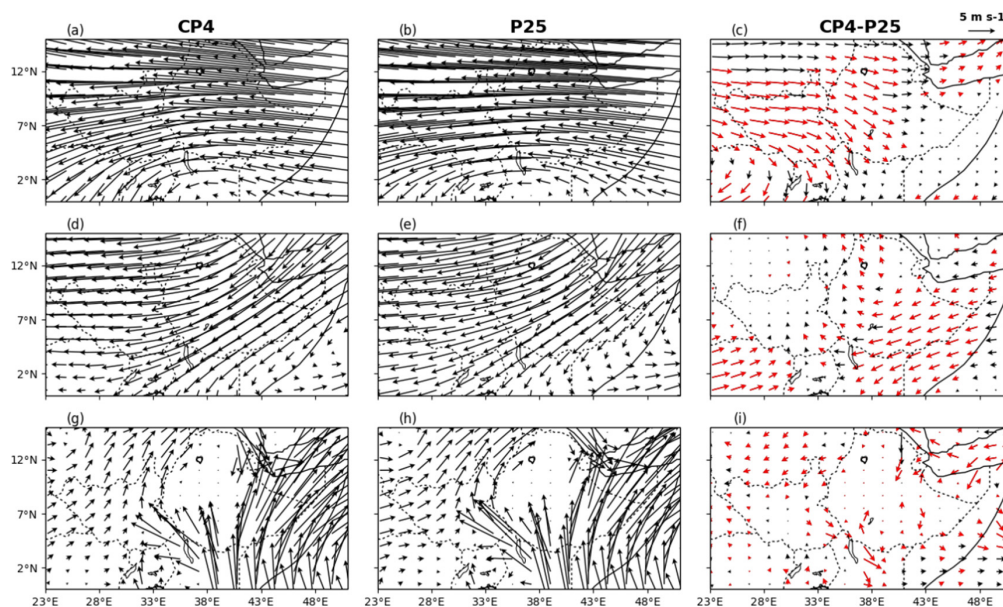

Figure 3. Climatology of July–August wind circulation over Ethiopia and S. Sudan in the CP4 current climate simulations from CP4 and P25 models, and the difference between CP4 and P25. The rows represent circulation patterns at 200 hPa (**a–c**), 500 hPa (**e–g**), and 850 hPa (**g–i**) levels, respectively. Red wind vectors represent regions with significant differences in u-wind or v-wind at the 5% limit based on Student's *t*-test applied to all July–August days in the climatology period.

Additionally, differences between CP4 and P25 are shown in Figure 3c,f,i. The TEJ is significantly weaker in the explicit model over Ethiopia, Sudan, S. Sudan, and the Red Sea region (Figure 3c). The Africa Easterly Jet (AEJ) in CP4 is similar to P25 over South Sudan and parts of Ethiopia, but significantly weaker in the south over Congo and significantly stronger in the east from southern Ethiopia to Somalia in the CP4 model (Figure 3f). This results in a greater convergence at 500 hPa around northern Uganda. At 850 hPa, there is a significantly weak Turkana Jet in CP4, as well as some subtle differences in the Somali Jet and low-level winds over Sudan which are statistically different from the P25 model (Figure 3i). The differences in TEJ and Turkana Jet stand out as particularly relevant regions for our study here.

3.2. Turkana Jet

Given the detailed orography in the Turkana channel, and the difference in orographic details in P25 and CP4 models, it is useful to take a more focused look at the Jet in this region to understand the impacts of detailed orographic information in regional climate simulations. Figure 4a,d shows spatial representation of winds in the region from CP4 and P25 models, while Figure 4b,e,c,f gives a snapshot of the winds using a transect parallel (perpendicular) to the Turkana jet core, respectively, as shown in Figure 1 (red and blue lines, respectively). Both models show the cross-equatorial flow from southern Indian Ocean is funneled through the Turkana channel, as a result of the geopotential gradient, to form the Turkana jet [23]. Broadly speaking, the two models have similar distributions of geopotential height at 900 hPa. However, P25 has relatively higher geopotential height near the East African coast compared to CP4, Figure 4a,d. This is a possible explanation for the weaker south easterlies (Turkana jet) in CP4 shown in Figure 3i.
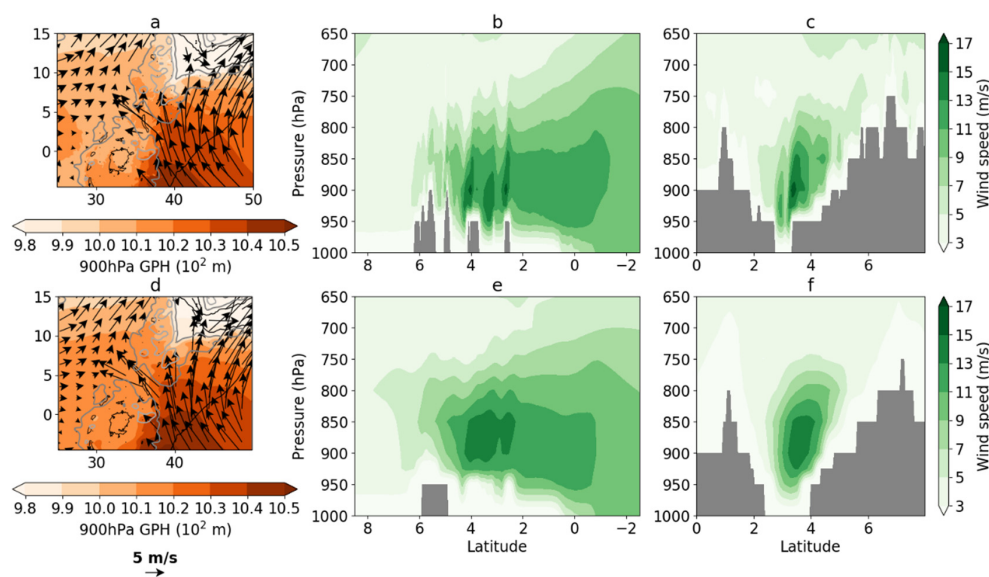

Figure 4. Geopotential height and wind vectors at 900 hPa in the region of the Turkana jet (**a**,**d**) and transects of wind speed parallel (**b**,**e**) and perpendicular (**c**,**f**) to the Turkana jet core (see Figure 1 for transects). Grey masking is applied where the pressure level is below the mean seasonal surface pressure. Simulations by CP4 (**a**–**c**; detailed orography) and P25 (**d**–**f**; less detailed orography). Both models are shown at their raw resolution. The difference in GPH and wind between CP4 and P25 is shown in the supplementary section, Figure S2.

Due to the resolved orography and the resulting dynamic effects in the CP4 model, the jet is broken into smaller cores than in the P25 model, when considering the parallel transect (Figure 4b,e). Similarly, from the perpendicular transect perspective (Figure 4c,f), P25 shows a broad core compared to smaller cores in the CP4 model. The detailed orography in CP4 appears to lead to the jet penetrating

less far into South Sudan, which is likely due to increased drag and frictional forces acting on the jet. Lack of orographic detail in climate models has been linked to biases in storm track, jet stream position, and blocking [55]. As far as we are aware this is the highest resolution version of the jet ever published, and given the strong role of orography, it is clear that the CP4 model provides useful simulations for understanding the climate of the region in the outflow of the Turkana jet.

3.3. Diurnal Cycle and Propagation of Rainfall Features

The diurnal cycle of rainfall and wind vector anomalies was analyzed at an interval of 3 h starting at 0000 UTC. However, for clarity, we only show a few snapshots of the analysis. Figure 5 shows the diurnal cycle of rainfall (shaded contours) and wind vector anomalies analyzed at 03, 09, 12, 15, 18, and 21 UTC. Wind anomalies were calculated as deviations of 3-h wind vectors from daily long-term mean. The two model outputs were validated against TRMM data. Results from TRMM data showed that convective activities occur predominantly in the afternoon peaking at 1200 UTC and for some places, such as western S. Sudan and Western Ethiopia, rainfall lasts late into the evening. TRMM data also captures the westward propagation of convective activities.
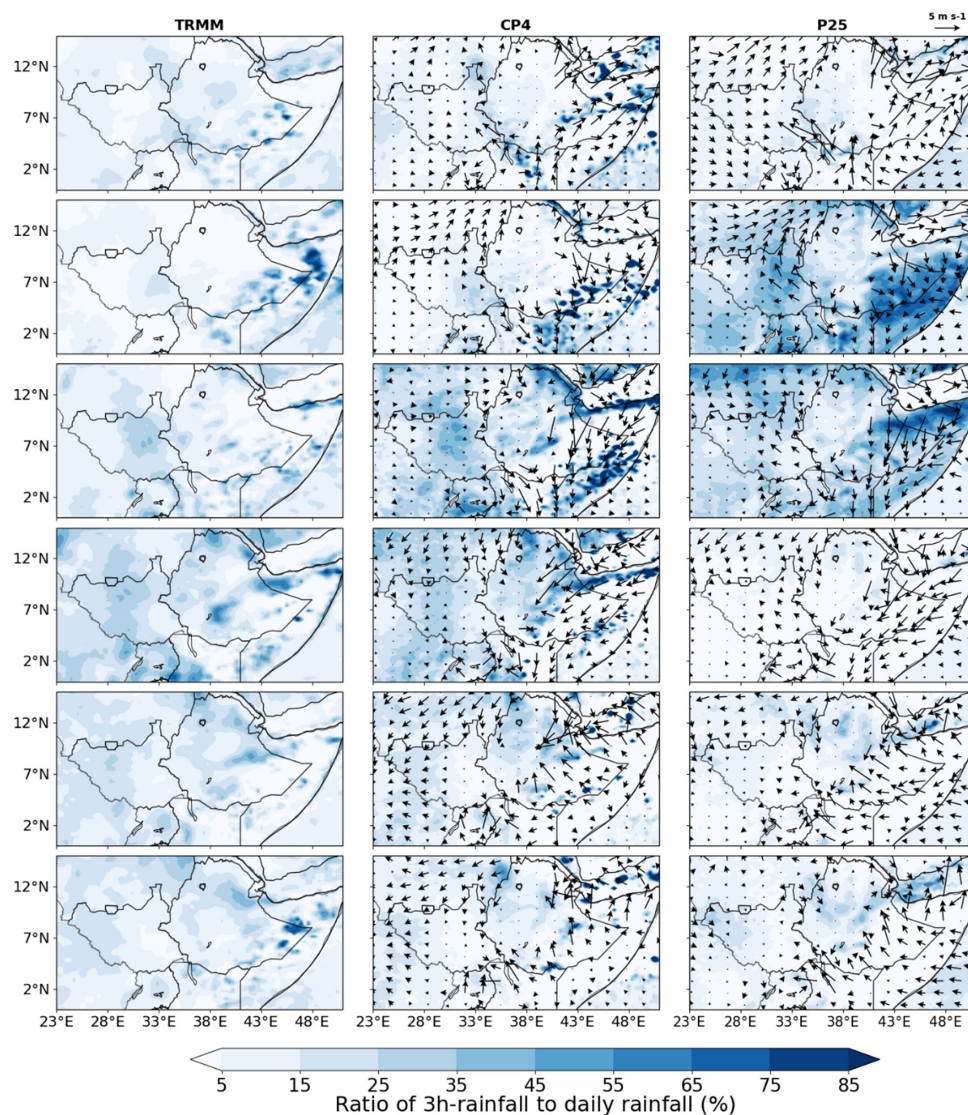
Figure 5. Diurnal cycle of wind anomalies (vectors) at 850 hPa level and percentage contribution of 3-h rainfall intensity to daily mean rainfall intensity (shaded) for TRMM, CP4 and P25 models (**left**, **middle** and **right** columns, respectively). The analysis is shown for 03, 09, 12, 15, 18, and 21 UTC (**top** to **bottom** rows, respectively).

The consistent westward shift in convective regions captured in TRMM is simulated by both models, however, CP4 simulation is more consistent with TRMM. Both models show consistency in simulating rainfall over Western Ethiopia region and north western South Sudan at 2100 UTC. Additionally, both models are able to simulate rainfall along the South Sudan–Ethiopia border region as well as along the Turkana channel at 0300 UTC. However, the differences in both models are more pronounced during daytime. The most obvious is the difference in timing of peak diurnal rainfall which is simulated at 0900 UTC and continues through to 1200 UTC in the P25 model while in the CP4 model, peak rainfall is simulated at 1200 UTC and continues late into the evening. The diurnal cycle of rainfall results from TRMM and CP4 are consistent with diurnal cycle of rainfall results during strong Turkana jet from [23], especially to the east of the jet exit region. It should be noted that south eastern Ethiopia, north eastern Kenya, and parts of Somalia are climatologically dry during this season (see Figure 2), however, all datasets showed high percentage contribution of rainfall in these areas. This is because any small amount of rainfall recorded in these areas is captured as an extreme event.

There is a strong diurnal variation in the low-level circulation in each model, which is linked to their rainfall, and slightly differs between the models. For example, there is increased horizontal convergence at 850 hPa level in the Turkana Outflow region at 0300 UTC in both models, but this is more pronounced in the P25 model. The convergence is as a result of strengthened low level westerlies and the Turkana Jet which is at its strongest at this time of day. Rainfall at this time is also associated with the strengthened Somali Low level jet. An abrupt large-scale increase in rainfall is observed in P25 at local midday (0900 UTC); however, this does not correspond to any major changes in dynamics in the P25 model. This is a well-known bias associated with parameterized convection simulations that is reduced in convection-permitting simulations [56].

In the afternoon (1200 UTC), the Turkana and Somali Jets are at their weakest in both models and this time also coincides with the time when diurnal rainfall peaks in CP4 model and begin to subside in P25 model. At 1500 UTC the low-level westerlies begin to weaken, and both the Somali and Turkana Jets are still weak, peak rainfall begins to subside in CP4, whilst a trace of rainfall is observed over few places in the P25 model. While the spatial patterns are similar at 1800 UTC between the two models, there is regeneration of rainfall in the P25 model while CP4 continues to register decrease in rainfall amount. There is similarity in the simulation of rainfall and winds at 2100 UTC in both models.

The westward propagating rainfall features originate from the Ethiopian highlands across South Sudan over the course of the day. In Figure 6, we use a Hovmöller to provide a clearer view of the west-to-east diurnal propagation and the skill of the models in capturing the propagating features. Similar propagation features were observed in both TRMM and CMORPH datasets especially the timing of centers of convective activities as they move from the highland regions 37.5° E westwards. Both satellite rainfall estimates show that afternoon rainfall begins at around 1200 UTC, with evening peaks at around 28° E (South Sudan), 35.5° (Western Ethiopian highlands), and 38° E (Eastern Ethiopian highlands). Rainfall propagates west from each peak with the eastern most reaching the western most in around 24 h (crossing the center of Box B, ≈30° E, at around 12 UTC). There is no major orographic trigger at 28° E (the mountains are further west at 25° E), so the afternoon/evening peak in rainfall there appears to be largely driven by local diurnal development of systems propagating from the west. Both CP4 and P25 are able to simulate night-time propagation of rainfall features but CP4 better propagates daytime rainfall features over the highlands into the night-time, and is better in the early morning. This is also confirmed by the high correlation-coefficient values of CP4 compared to P25 model (CP4 > 0.7 vs. P25 < 0.2). Additionally, P25 shows a strong peak across all longitudes at local midday, and does not capture the peak at 15 UTC and 28° E, supporting the hypothesis that propagation is important for this peak.
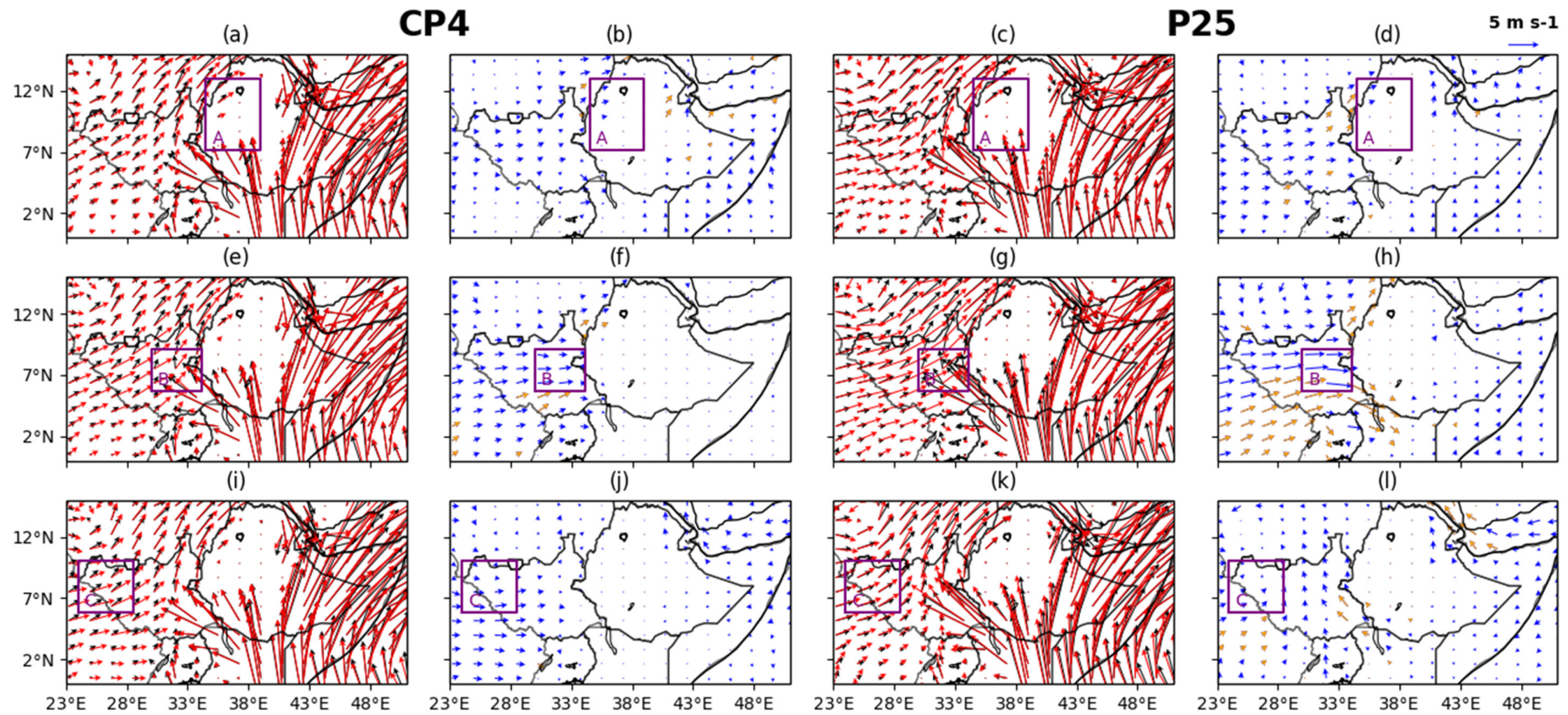
3.4. Dynamics Associated with Extreme Rainfall

Next, we considered the role of circulation in generating extreme rainfall. This analysis was based on three subregions (Western Ethiopia, Turkana Outflow, and western South Sudan) which are shown in

Figure 1 and are, respectively, presented as boxes A, B, C (or rows) in Figure 7. Columns 1 and 3 represent analysis based on the absolute mean wind on all July–August days (red vectors) superimposed on mean wind for the wettest 5% of 1997–2007 July–August days (black vectors), while columns 2 and 4 represent the anomalies (blue vectors) and their significance (orange vectors) taken as the difference between the composites (black vectors) and mean wind fields (red vectors) for CP4 and P25 models.
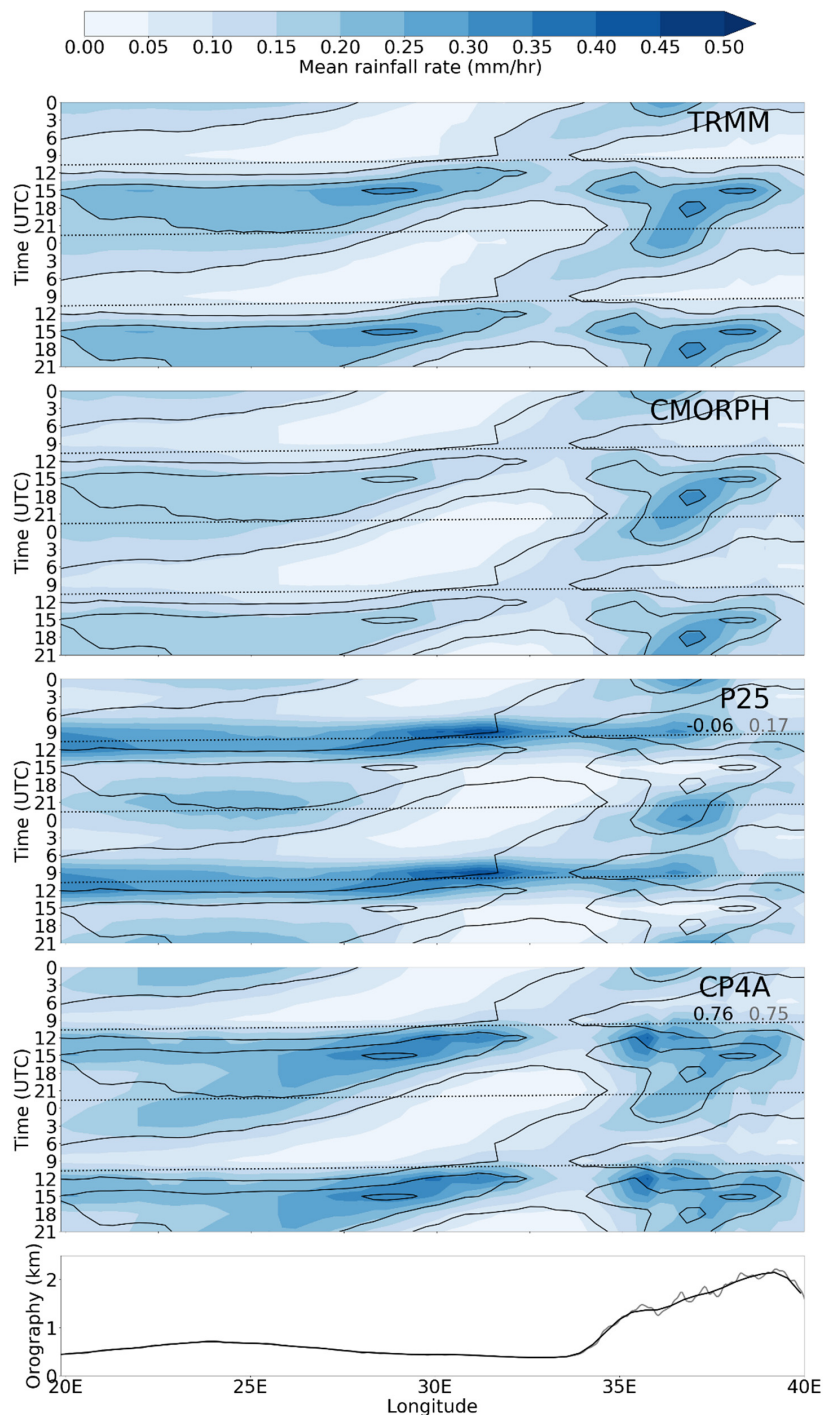
Figure 6. Hovmöller of rainfall diurnal climatology mean over 5° to 10° latitude for the two satellite rainfall products and for CP4 and P25. Red contour repeats the TRMM contours on the other panels. Bottom panel shows the mean orography of the P25 grid (black) and the CP4 grid (grey). Dotted lines on Hovmöller plots indicate local midday and midnight. Black (grey) values represent Pearson correlation coefficient of the model Hovmöller against TRMM (black value) and CMORPH (grey value). Only CP4 values are significant at the 5% level.

Figure 7. Mean dynamics and the dynamic anomalies at 850 hPa associated with extreme rainfall over selected regions (Western Ethiopia, (**a**–**d**); Turkana Outflow, (**e**–**h**); Western S. Sudan, (**i**–**l**); represented by boxes A, B, and C, respectively) for the current climate. The red, black, and blue wind vectors represent the wind climatology, wind composite during extreme wet days, and composite minus climatology, respectively. The threshold for extreme rainfall used was the 95th percentile of all days. Orange wind vectors represent regions with significant changes in u-wind or v-wind at the 5% limit based on Welch's *t*-test applied to all July–August days in the climatological period and on extreme wet days.

The influx of moisture into this region is expected from the west; the Congo basin and Atlantic Ocean [4] through increased low-level westerlies. Increased moisture influx is expected in both models as illustrated by increased low-level westerlies, especially for the composite dynamics based on extreme precipitation in W. Ethiopia and Turkana Outflow regions (Figure 7b,d,f,h). The intensification of the low-level westerlies is statistically significant in both CP4 and P25 models in southern S. Sudan. Extreme precipitation in Western Ethiopia is also associated with an intensified Somali jet in both models (Figure 7b,d).

However, key differences were noticeable especially in the P25 simulations. Firstly, P25 has relatively stronger westerly anomalies during extreme rainfall days, a difference that is not seen in the mean low-level westerlies (Figure 3). Secondly, P25 shows stronger anomalies in the Turkana jet during extremely wet days: it has a significantly weaker jet on extremely wet days in the Turkana outflow region (Figure 7h) and significantly stronger jet on days with extreme rainfall in western South Sudan (Figure 7l). This is consistent with [23] analysis of reanalyzed winds and mean observed rainfall. It is not seen in CP4A and it is not clear if this is a deficiency of the convection-permitting simulation, or if the reanalyzed winds used by [23] are biased, along with the P25 model here. Such a bias of the reanalysis may be expected since there are few observations in the region so reanalysis winds are poorly constrained, and instead will be left to the model physics to simulate. In this case, the reanalysis model will have a coarser representation of orography and parametrized convection compared to CP4, and therefore may be expected to be more similar to our P25 model.

Circulation patterns at higher levels (200 hPa level) indicate that extremely wet days over western Ethiopia in both P25 and CP4 models seem to respond to an enhanced Tropical Easterly Jet (Figure 8b,d) [4,9,17], but a significantly stronger zonal anomaly is present in the CP4 in a few parts of Sudan and Ethiopia in the CP4 model. Another similarity in the models is on the composite dynamics based on western South Sudan extreme rainfall which seem to respond to a weaker Tropical Easterly jet (Figure 8j,l). This signal is significant over central parts of South Sudan in both models and off the coast of Somalia in the P25 model (Figure 8l). Considering this result (Figure 8) in combination with the result in Figure 7, suggests that the extreme rainfall in CP4 may respond more strongly to the vertical wind shear driving storms than P25, and P25 responds more strongly to variations in low-level westerlies. The response to low-level westerlies likely highlights a strong control of low-level moisture in the P25 model. This relationship is consistent with the finding that storms simulated with explicit convection respond directly to the effect of shear to intensify the storm [57,58]. The results based on extreme rainfall in the Turkana Outflow region were distinct; for example, the anomalous wind divergence and wind patterns exhibited by upper level winds in Figure 8f are different from Figure 8h. This is likely a consequence, not a cause, of the extreme rainfall and presence of deep convection.
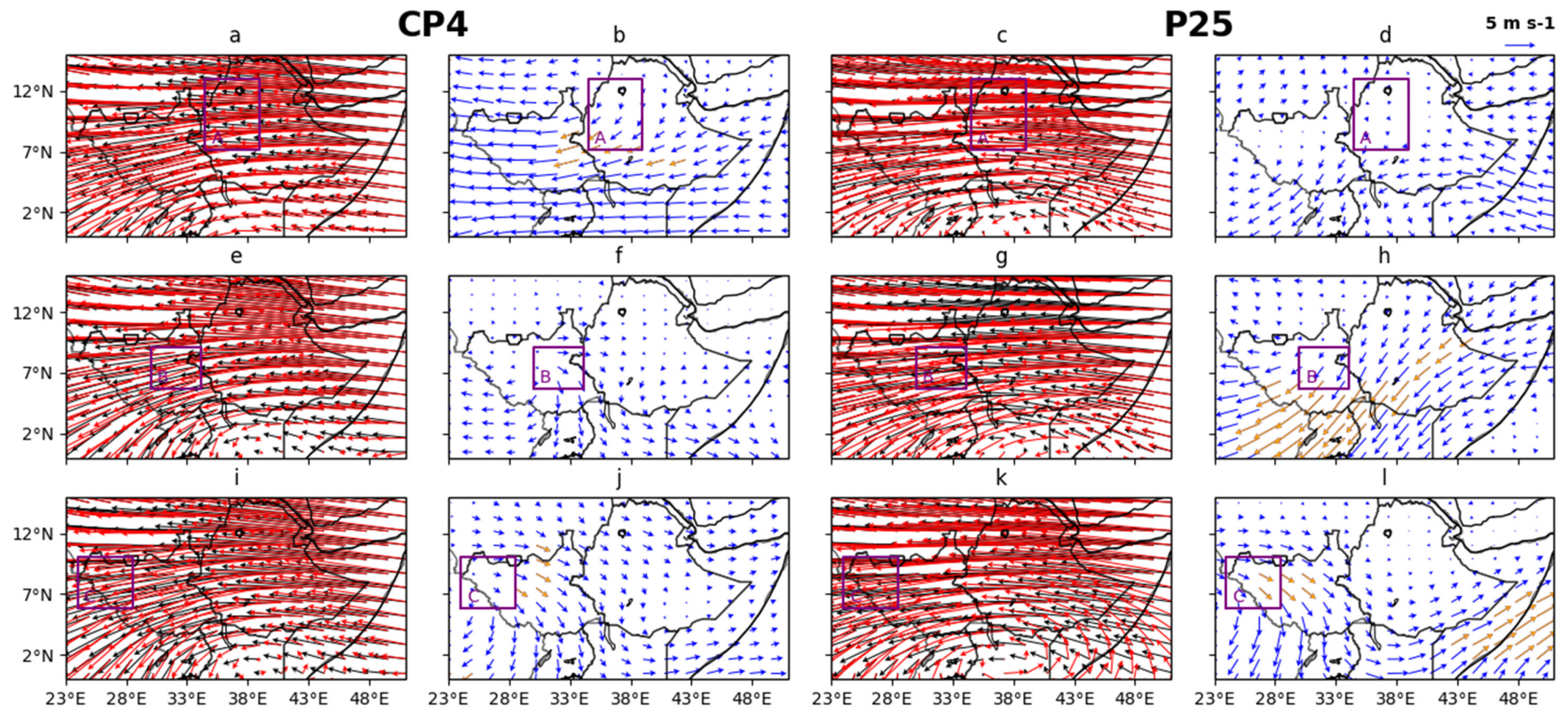
Figure 8. Same as Figure 7 but for the dynamics at upper (200 hPa) level.

3.5. Projected End-of-Century Changes in Rainfall and Dynamics

Figure 9 shows the projected future mean changes of rainfall metrics by the end of 21st under a business-as-usual scenario as simulated by CP4 and P25 models. Similar to Figure 2, four metrics (mean July–August rainfall, mean wet day intensity, number of wet days, and 95th percentile of rainfall) were used to analyze the future changes in rainfall characteristics.
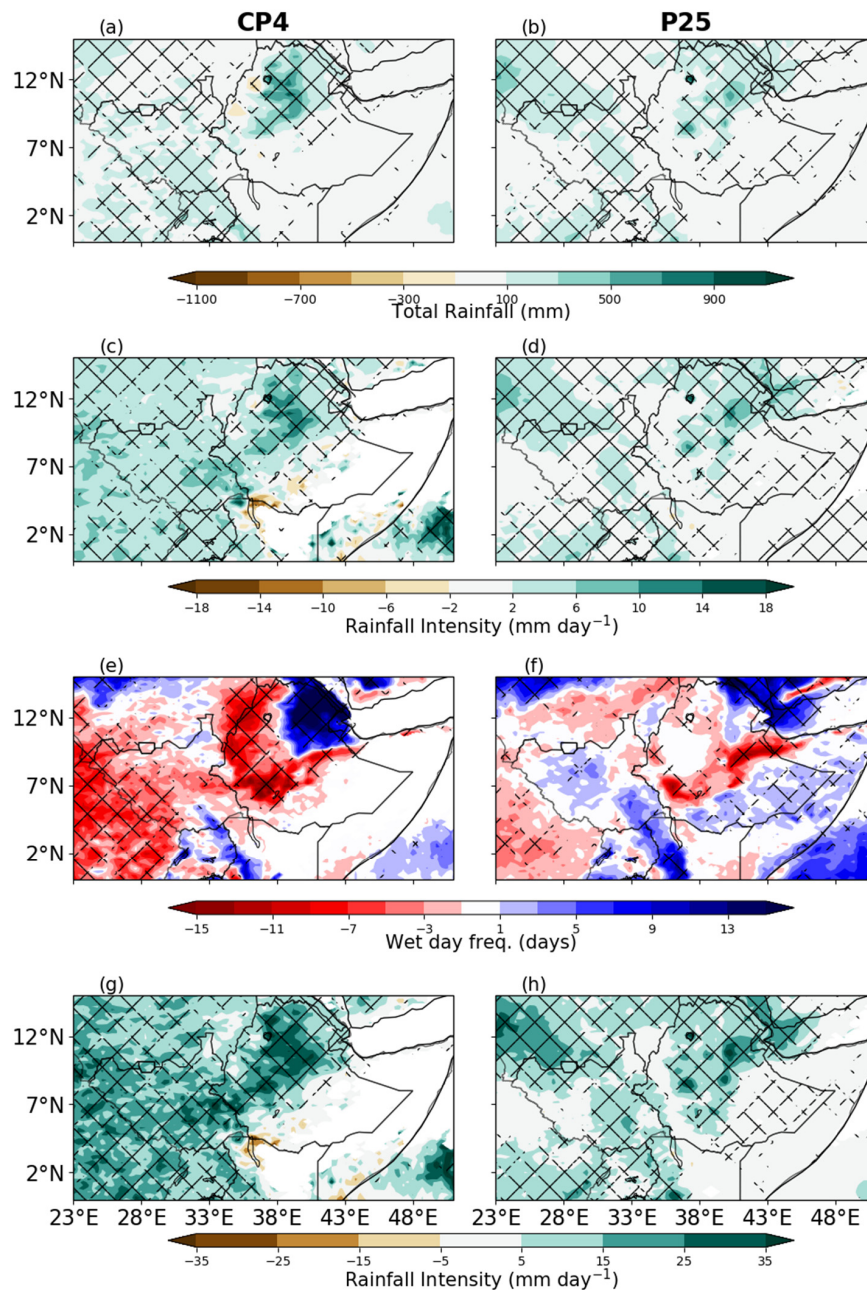
Figure 9. Projected changes (future climate minus current climate) in mean seasonal rainfall (**a**,**b**), mean wet day intensity (**c**,**d**), mean frequency of wet days (**e**,**f**), and mean extreme (95th percentile) wet day intensity (**g**,**h**) for both CP4 and P25 models. The means are calculated for July–August over the period of simulation in both historical and future simulations. Hatches show significant grid cells at the 5% limit based on the Student's *t*-test applied to all July–August days in the climatological periods and Welch's *t*-test applied to all July–August extremely wet days in the climatological periods. A similar figure showing the projected percent change in the rainfall indices is included in the supplementary section, Figure S3.

From Figure 9(a,b), both models simulate a significant increase in future mean total seasonal rainfall (July–August) over the Ethiopian highlands with CP4 simulating the highest increase of up to 900 mm. The wet day intensity (Figure 9c,d) is also projected to significantly increase by at least 2 mm per day on average in most parts of the region in both models. However, the CP4 run simulated high intensity rainfall on average over a much larger area west of the Rift Valley compared to the P25 for which high intensity rainfall areas exceeding 6 mm/day were limited to isolated areas over central Rift Valley and surrounding highlands. Since the CP4 model is explicitly representing the physics of storms, and the response of storm dynamics to climate change [37,40], it provides some level of confidence in its larger simulated response of rainfall intensity to climate change. However, this confidence is still limited due to different sources of uncertainties. One source of uncertainty is the model physics within convection-permitting simulations, which still require further assessments of their applicability, especially at the convection permitting scales [59]. The other source of uncertainty is the number of simulations/multimodel runs. For example, traditional treatment of turbulence using approximations such as Reynolds averaging are not valid at the microscale [59].

The CP4 run simulated a significantly larger and more widespread drop, than the P25 model, in the number of wet days over much of Ethiopia and South Sudan (Figure 9e,f). Conversely, a significant increase in wet day frequency is projected north of Ethiopia, and in Eritrea as well as Djibouti defining a SW–NE dipole feature over western Ethiopia in the CP4 model run. The region of significant increase in wet day frequency is shifted farther northwards in the Suez Canal region in P25. Even though a dipole feature (increase/decrease of wet day frequency) is still discernible in the P25 simulation, it is weaker over the Ethiopia/South Sudan region than the CP4 simulation. Despite not being the main season in south eastern Ethiopia, northern Kenya and Somalia, P25 model projects a slight increase (up to 5 days increase in some areas) in wet day frequency which is not the case in CP4.

The future spatial distribution of change in extreme wet day intensity are similar in CP4 and P25 models, in which both models projected significant increase in wet day intensity over much of western Ethiopia and S. Sudan. However, the increase is larger and more widespread in the CP4 than P25 model. There is a dipole feature (decrease/increase in extreme rainfall near the jet entrance/exit region) projected at the vicinity of the Turkana jet in the CP4 model similar to that of projected changes in wet day intensity in the same model, Figure 9g. This dipole feature is not visible in the P25 simulations, Figure 9h. Generally, the parameterized model projects significant changes in all metrics in regions, such as south eastern Ethiopia and Somalia, where the JA season is not significant based on current observations.

From the analysis it is apparent that even though the projected future rainfall days could decrease over most parts of the region, for total rainfall this will be compensated by the increased mean and extreme rainfall intensity. This explains the projected increase in seasonal mean rainfall. As we showed in Figure 2, both intensity and frequency of rainfall are better simulated in current climate by CP4. Therefore, the relatively low skill in the parametrized convection model, compared to the convection-permitting model, should act as a warning regarding the reliability of global and regional climate model projections using parametrized convection simulations in the region.

The future changes in the dynamics and regions of significant changes (red wind vectors) at three pressure levels (850, 500, and 200 hPa) for CP4 and P25 models are presented in Figure 10. At lower levels (850 hPa) significant strengthening of the westerlies is projected over South Sudan and Sudan in both models, Figure 10e,f. The Somali low-level jet at 850 hPa is projected to be weaker in the future by both models, but with a larger reduction in the P25 model. At the 500 hPa level, the CP4 model shows significant strengthening of the AEJ over South Sudan and Sudan, not apparent in P25 which instead only shows a slight strengthening in the north of the domain, Figure 10c,d. The future changes in upper level winds (200 hPa) indicate that easterlies will likely be weaker in south western South Sudan in CP4 where the changes are negligible, Figure 10a. Similar patterns were observed in P25 except that the changes were relatively stronger (Figure 10b).
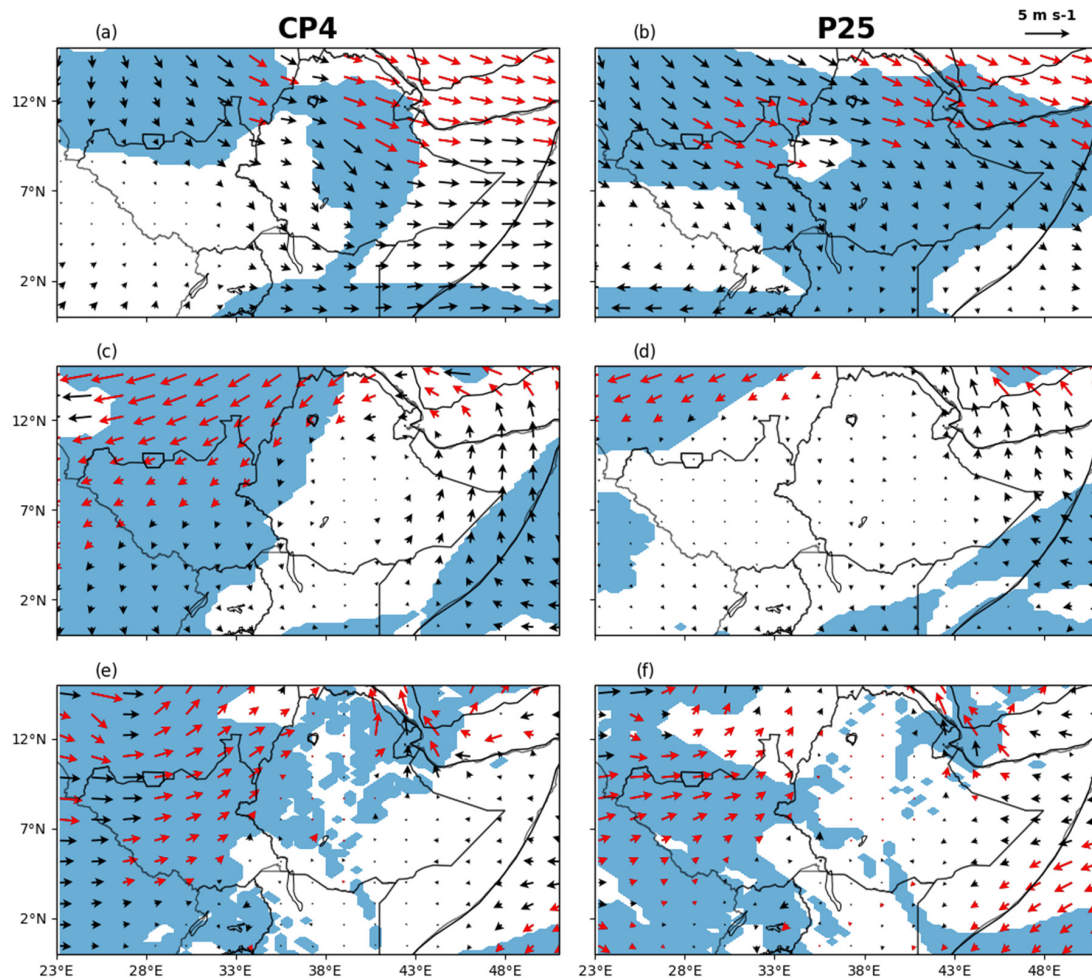
Figure 10. Future changes in the dynamics for CP4 and P25 models at three pressure levels, 200 hPa (**a**,**b**), 500 hPa (**c**,**d**), and 850hPa (**e**,**f**). Red wind vectors represent regions with significant changes in u-wind or v-wind at the 5% limit based on the Student's *t*-test applied to all July–August days in the climatological period. Shading (in blue) show regions with more than 50% change (absolute change between future and current climate expressed as percentage) in either u-wind or v-wind.

The significant increase in low level westerlies shown in Figure 10 will likely bring in additional moisture into the region to drive the increase in the intensity of wet (Figure 9) days by end of century in both models. A weaker TEJ over Ethiopia may explain the reduction in the number of wet days through the reduction in the vertical wind shear. Strong vertical wind shear can aid in the development of convective storms either through development of new convective cells along the boundary of the storm-induced cold outflow near the surface or through the splitting of the storm into a pair of self-sustaining cells [60].

3.6. Projected End-of-Century Changes in Turkana Jet

Figure 11 shows the projected changes in the geopotential height and winds in the vicinity of the Turkana jet. Figure 11a shows that there is a general increase in geopotential height across the region. However, there is a relatively larger increase in the geopotential heights over the ocean which results in an increase in pressure gradient force. The center of the future increase in geopotential height is shifted northwards compared to current climate simulation (Figure 4). This projected feature results in the weakening of the Somali Jet and a strengthening of the Turkana Jet. In the current climate, the differences in geopotential height along the Turkana channel is different by only 1.5 m between CP4 and P25 (Figure 11d). In the future climate, the difference in the 900 hPa geopotential height through

the channel is bigger in CP4 (Figure 11d) which could, additionally, explain the small increase in wind speed within the channel at 900 hPa in CP4, but with little change in the P25 simulation. The results also show that the jet core may shift towards lower levels, with increases in wind speeds changes occurring at approximately 950 hPa in both models, and decreases at 750 hPa. This is a consistent feature in both models suggesting the result is independent of the representation of convection or resolution.
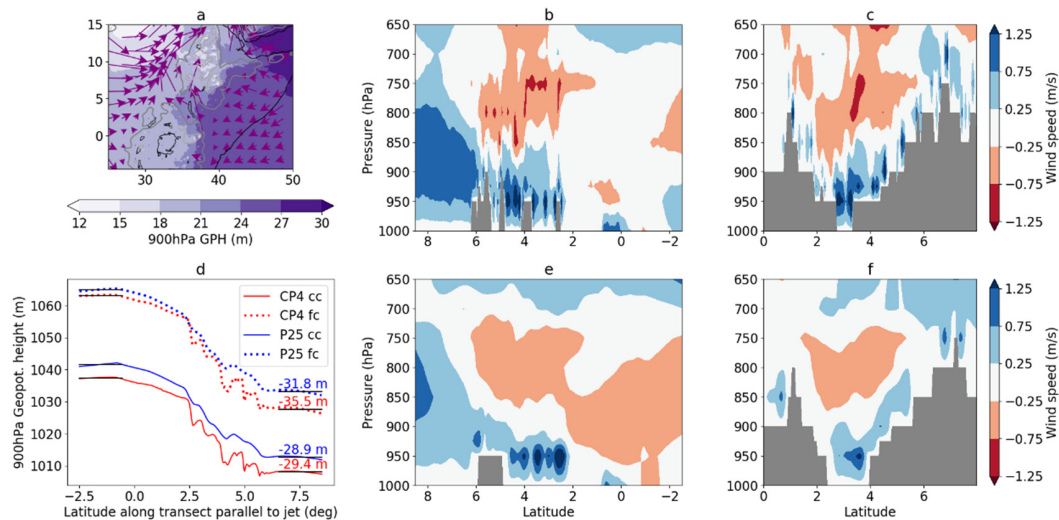
Figure 11. Change in geopotential height and wind vectors between current and future climate at 900 hPa in the region of the Turkana jet (**a**), differences in 900 hPa geopotential height in current and future climate along transect parallel to Turkana jet (**d**), and transects of wind speed parallel (**b**,**e**) and perpendicular (**c**,**f**) to the Turkana jet core (see Figure 1). The simulations by CP4 (**a**–**c**; detailed orography) and P25 (**e**–**f**; less detailed topography) are shown at their raw resolutions.

Figure 4 showed that the jet core was located around 900 hPa, but at this level there is less change in both models. CP4 shows the largest changes and this may relate to the stronger increase in 900 hPa geopotential height gradient in CP4 compared to P25. Despite the indications that jet core may not substantially change in future, the potential for increased winds at low levels is of much interest for wind farms in the region. The energy available to wind turbines is proportional to the wind speed cubed. A preliminary analysis was undertaken of the windspeed cubed at a height of ≈100 m above the surface, and interpolated to 36.8E, 2.5N (approximately the location of an existing wind farm in the Turkana channel). For this future scenario the CP4 and P25 models show an average increase in wind speed cubed, over the whole year, of 8% and 24%, respectively. CP4 mean wind speed cubed was regridded to the same horizontal grid as P25 before calculating the percentage change. Our results suggest that there may be a modest increase in wind energy in the Turkana channel under climate change, though the smaller increase was found with the model with better simulation of the terrain. Nevertheless, this is an interesting result that encourages further study, which is required to make a robust statement since our study uses a single model, time slice, and scenario and also does not consider potential changes in land-use or aerosols which could have other effects on low-level winds.

4. Summary and Conclusions

This study sought to assess the circulation patterns linked to current and projected rainfall over Ethiopia and South Sudan from two models: one which allows convection to explicitly develop (CP4) and the other that parameterizes convection (P25). Comparing the two models gives us insight how commonly used models such as those in the Coupled Model Intercomparison Project (CMIP) and Coordinated Regional Downscaling Experiment (CORDEX) ensembles, and which all parametrize moist convection, may be limited by convection parametrization. Analysis focused on two main areas:

(i) rainfall and circulation patterns in the current climate and (ii) future changes in these parameters at the end of the century under a high-end business-as-usual scenario.

The domain of study was Eastern Africa with a focus on Ethiopia and South Sudan. Three additional subregions were defined (Western Ethiopia, Turkana Outflow, and Western South Sudan) to aid with the analysis of extreme rainfall events. The analysis was done at subdaily, daily, and seasonal time-scales mainly focusing on the peak rainfall months (July–August) for much of Ethiopia and South Sudan.

In the current climate, the models were evaluated using two satellite rainfall products, TRMM and CMORPH. Evaluation of rainfall showed that CP4 model is relatively skillful in capturing wet day frequency distribution, and better than P25 for this and for 'intense rainfall' (the 95th percentile of rainfall on wet days). Both models showed some night-time rainfall propagation through South Sudan but only CP4 showed a strong correlation with satellite rainfall products for the full diurnal cycle and propagation (CP4: >0.7, P25: <0.2).

Low-level westerlies play a key role on the days with extreme rainfall in both models, but this is more pronounced in P25, perhaps as its rainfall is more sensitive to low-level moisture, whereas convergence and vertical wind shear can provide additional controls on convection in the CP4 model. A difference between the models also arose in the response of extreme rainfall days to changes in the Turkana jet, with the P25 model showing a weakening of the jet on such days, whilst the CP4 model showed little change. The increased orographic detail present in the CP4 model introduced additional details in the Turkana jet not present in the P25 model, and reduced its extent into South Sudan. Therefore, this high-resolution model draws into question the influence of the jet on extreme rainfall over South Sudan. More observations in the region are imperative, in order to understand this feature. Overall, the results from current climate have shown that simulation of regional climate using convection permitting methods can significantly improve the timing of convection, frequency distribution of extreme rainfall, and a more detailed representation of circulation features especially the Turkana jet.

Projected seasonal (July–August) mean rainfall increased over most parts of the domain by the end of 21st century in both models. This occurred despite the projected decrease in the number of wet days, as there was an even greater projected increase in the wet day rainfall intensity. Extreme rainfall is projected to increase in both models, with much greater and more widespread increases seen in CP4.

Consistent with the projected rainfall increases, there is also a projected increase in the low-level westerlies in both models. Further, both models showed a shift of the Turkana jet to lower levels, showing that this result is independent of the representation of convection or resolution in the future climate. The P25 model shows very few areas with significant changes in wet days. On the contrary, CP4 mode shows significant changes in the wet day frequency over large regions. Notably, increases in northern Ethiopia, and decreases in western Ethiopia. On the contrary, the spatial patterns of the changes in the mean wet day and extreme wet day intensity projected by the explicit model resembled a dipole pattern at the Turkana jet entrance/exit region. Further, the dipole pattern in the changes in extreme rainfall at the Turkana jet entrance/exit region in CP4 model may result from the stronger change in the Turkana jet indicating that CP4 is responding more realistically to convergence than a parametrized model [32].

In conclusion, the study has shown the value of convection permitting model (CP4) in simulating convection and circulation patterns in a tropical region defined by complex terrain and organized propagating convective systems. Substantial benefits were demonstrated in simulation of the diurnal cycle, frequency, and intensity of rainfall. The greater and more widespread climate change in extreme rainfall in CP4 shows a major limitation of using only CMIP and CORDEX models for informing decisions depending on climate change in the region.

rainfall indices between current and end-of-century climates for CP4 and P25 models. Masked areas (in grey) represent areas which receive total rainfall amount less than 10mm during July-August**.**

References

1.　United Nations Office for Disaster Risk Reduction (UNISDR) and Internal Displacement Monitoring Centre (IDMC). *Displacement in the Greater Horn of Africa: A Disaster Risk Reduction Perspective*; United Nations Office for Disaster Risk Reduction (UNISDR) and Internal Displacement Monitoring Centre (IDMC): Nairobi, Kenya, 2017.

2.　Isaac, I.I. *Inter-African Development and Development Fund (IADF): With Alternative Strategies towards Sustainable Economic Development for Africa*; Trafford Publishing: Bloomington, IN, USA, 2009.

3.　Vijverberg, J.; Sibbing, F.A.; Dejen, E. Lake Tana: Source of the Blue Nile. In *The Nile*; Springer: Dordrecht, The Netherlands, 2009; pp. 163–192.

4.　Segele, Z.T.; Lamb, P.J. Characterization and variability of Kiremt rainy season over Ethiopia. *Meteorol. Atmos. Phys.* **2005**, *89*, 153–180. [CrossRef]

5.　Korecha, D.; Barnston, A.G. Predictability of June–September Rainfall in Ethiopia. *Mon. Weather Rev.* **2007**, *135*, 628–650. [CrossRef]

6.　Segele, Z.T.; Lamb, P.J.; Leslie, L.M. Seasonal-to-Interannual Variability of Ethiopia/Horn of Africa Monsoon. Part I: Associations of Wavelet-Filtered Large-Scale Atmospheric Circulation and Global Sea Surface Temperature. *J. Clim.* **2009**, *22*, 3396–3421. [CrossRef]

7.　Nicholson, S.E. Climate and climatic variability of rainfall over eastern Africa. *Rev. Geophys.* **2017**, *55*, 590–635. [CrossRef]

8.　Hartman, A.T. An analysis of the effects of temperatures and circulations on the strength of the low-level jet in the Turkana Channel in East Africa. *Theor. Appl. Climatol.* **2018**, *132*, 1003–1017. [CrossRef]

9.　Nicholson, S.E. The Turkana low-level jet: Mean climatology and association with regional aridity. *Int. J. Climatol.* **2016**, *36*, 2598–2614. [CrossRef]

10.　Segele, Z.T.; Lamb, P.J.; Leslie, L.M. Large-scale atmospheric circulation and global sea surface temperature associations with Horn of Africa June-September rainfall. *Int. J. Climatol.* **2009**, *29*, 1075–1100. [CrossRef]

11.　Williams, A.P.; Funk, C.C.; Michaelsen, J.; Rauscher, S.A.; Robertson, I.; Wils, T.H.G.; Koprowski, M.; Eshetu, Z.; Loader, N.J. Recent summer precipitation trends in the Greater Horn of Africa and the emerging role of Indian Ocean sea surface temperature. *Clim. Dyn.* **2012**, *39*, 2307–2328. [CrossRef]

12.　Viste, E.M.; Sorteberg, A. Moisture transport into the Ethiopian highlands. *Int. J. Climatol.* **2013**, *33*, 249–263. [CrossRef]

13.　Viste, E.M.; Sorteberg, A. The effect of moisture transport variability on Ethiopian summer precipitation. *Int. J. Climatol.* **2013**, *33*, 3106–3123. [CrossRef]

14.　Camberlin, P.; Fontaine, B.; Louvet, S.; Oettli, P.; Valimba, P. Climate Adjustments over Africa Accompanying the Indian Monsoon Onset. *J. Clim.* **2010**, *23*, 2047–2064. [CrossRef]

15. Beltrando, G.; Camberlin, P. Interannual variability of rainfall in the eastern horn of Africa and indicators of atmospheric circulation. *Int. J. Climatol.* **1993**, *13*, 533–546. [CrossRef]

16. Zeleke, T.; Giorgi, F.; Tsidu, G.M.; Diro, G.T. Spatial and temporal variability of summer rainfall over Ethiopia from observations and a regional climate model experiment. *Theor. Appl. Climatol.* **2013**, *111*, 665–681. [CrossRef]

17. Segele, Z.T.; Leslie, L.M.; Tarhule, A. Sensitivity of Horn of Africa Rainfall to Regional Sea Surface Temperature Forcing. *Climate* **2015**, *3*, 365–390. [CrossRef]

18. Shongwe, M.E.; Van Oldenborgh, G.J.; van den Hurk, B.; Van Aalst, M. Projected Changes in Mean and Extreme Precipitation in Africa under Global Warming. Part II: East Africa. *J. Clim.* **2011**, *24*, 3718–3733. [CrossRef]

19. Otieno, V.O.; Anyah, R.O. CMIP5 simulated climate conditions of the Greater Horn of Africa (GHA). Part II: Projected climate. *Clim. Dyn.* **2013**, *41*, 2099–2113. [CrossRef]

20. Endris, H.S.; Omondi, P.; Jain, S.L.; Lennard, C.; Hewitson, B.; Chang'A, L.; Awange, J.L.; Dosio, A.; Ketiem, P.; Nikulin, G.; et al. Assessment of the Performance of CORDEX Regional Climate Models in Simulating East African Rainfall. *J. Clim.* **2013**, *26*, 8453–8475. [CrossRef]

21. Osima, S.; Indasi, V.S.; Zaroug, M.; Endris, H.S.; Gudoshava, M.; Misiani, H.O.; Nimusiima, A.; Anyah, R.O.; Otieno, G.; Ogwang, B.A.; et al. Projected climate over the Greater Horn of Africa under 1.5 °C and 2 °C global warming. *Environ. Res. Lett.* **2018**, *13*, 065004. [CrossRef]

22. Endris, H.S.; Lennard, C.; Hewitson, B.; Dosio, A.; Nikulin, G.; Artan, G.A. Future changes in rainfall associated with ENSO, IOD and changes in the mean state over Eastern Africa. *Clim. Dyn.* **2018**, *52*, 2029–2053. [CrossRef]

23. Vizy, E.K.; Cook, K.H. Observed relationship between the Turkana low-level jet and boreal summer convection. *Clim. Dyn.* **2019**, *53*, 4037–4058. [CrossRef]

24. Kinuthia, J.H. Horizontal and Vertical Structure of the Lake Turkana Jet. *J. Appl. Meteorol.* **1992**, *31*, 1248–1274. [CrossRef]

25. Kinuthia, J.H.; Asnani, G.C. A Newly Found Jet in North Kenya (Turkana Channel). *Mon. Weather Rev.* **1982**, *110*, 1722–1728. [CrossRef]

26. Crook, J.A.; Klein, C.; Folwell, S.; Taylor, C.M.; Parker, D.J.; Stratton, R.; Stein, T.H.M. Assessment of the Representation of West African Storm Lifecycles in Convection-Permitting Simulations. *Earth Space Sci.* **2019**, *6*, 818–835. [CrossRef]

27. Taylor, C.M.; Belušić, D.; Guichard, F.; Parker, D.J.; Vischel, T.; Bock, O.; Harris, P.P.; Janicot, S.; Klein, C.; Panthou, G. Frequency of extreme Sahelian storms tripled since 1982 in satellite observations. *Nature* **2017**, *544*, 475–478. [CrossRef] [PubMed]

28. Marsham, J.H.; Dixon, N.S.; Garcia-Carreras, L.; Lister, G.M.S.; Parker, D.J.; Knippertz, P.; Birch, C.E. The role of moist convection in the West African monsoon system: Insights from continental-scale convection-permitting simulations. *Geophys. Res. Lett.* **2013**, *40*, 1843–1849. [CrossRef]

29. Pearson, K.; Lister, G.M.S.; Birch, C.E.; Allan, R.P.; Hogan, R.J.; Woolnough, S.J. Modelling the diurnal cycle of tropical convection across the 'grey zone'. *Q. J. R. Meteorol. Soc.* **2013**, *140*, 491–499. [CrossRef]

30. Stein, T.H.M.; Parker, D.J.; Hogan, R.J.; Birch, C.E.; Holloway, C.E.; Lister, G.M.S.; Marsham, J.H.; Woolnough, S.J. The representation of the West African monsoon vertical cloud structure in the Met Office Unified Model: An evaluation with CloudSat. *Q. J. R. Meteorol. Soc.* **2015**, *141*, 3312–3324. [CrossRef]

31. Finney, D.L.; Marsham, J.H.; Jackson, L.S.; Kendon, E.J.; Rowell, D.P.; Boorman, P.M.; Keane, R.J.; Stratton, R.A.; Senior, C.A. Implications of Improved Representation of Convection for the East Africa Water Budget Using a Convection-Permitting Model. *J. Clim.* **2019**, *32*, 2109–2129. [CrossRef]

32. Birch, C.E.; Marsham, J.H.; Parker, D.J.; Taylor, C.M. The scale dependence and structure of convergence fields preceding the initiation of deep convection. *Geophys. Res. Lett.* **2014**, *41*, 4769–4776. [CrossRef]

33. Wainwright, C.M.; Marsham, J.H.; Rowell, D.P.; Finney, D.L.; Black, E. Future changes in seasonality in Eastern Africa from regional simulations with explicit and parametrised convection. *J. Clim.* **2020**, 1–54. [CrossRef]

34. Stratton, R.; Senior, C.A.; Vosper, S.B.; Folwell, S.S.; Boutle, I.A.; Earnshaw, P.D.; Kendon, E.; Lock, A.P.; Malcolm, A.; Manners, J.; et al. A Pan-African Convection-Permitting Regional Climate Simulation with the Met Office Unified Model: CP4-Africa. *J. Clim.* **2018**, *31*, 3485–3508. [CrossRef]

35. Walters, D.; Boutle, I.; Brooks, M.; Melvin, T.; Stratton, R.; Vosper, S.B.; Wells, H.; Williams, K.; Wood, N.; Allen, T.; et al. The Met Office Unified Model Global Atmosphere 6.0/6.1 and JULES Global Land 6.0/6.1 configurations. *Geosci. Model Dev.* **2017**, *10*, 1487–1520. [CrossRef]

36. Finney, D.L.; Marsham, J.H.; Rowell, D.P.; Kendon, E.J.; Tucker, S.O.; Stratton, R.A.; Jackson, L.S. Effects of Explicit Convection on Future Projections of Mesoscale Circulations, Rainfall, and Rainfall Extremes over Eastern Africa. *J. Clim.* **2020**, *33*, 2701–2718. [CrossRef]

37. Fitzpatrick, R.G.J.; Parker, D.J.; Marsham, J.H.; Rowell, D.P.; Guichard, F.M.; Taylor, C.M.; Cook, K.H.; Vizy, E.K.; Jackson, L.S.; Finney, D.; et al. What Drives the Intensification of Mesoscale Convective Systems over the West African Sahel under Climate Change? *J. Clim.* **2020**, *33*, 3151–3172. [CrossRef]

38. Berthou, S.; Kendon, E.J.; Chan, S.C.; Ban, N.; Leutwyler, D.; Schär, C.; Fosser, G. Pan-European climate at convection-permitting scale: A model intercomparison study. *Clim. Dyn.* **2020**, *55*, 35–59. [CrossRef]

39. Jackson, L.S.; Finney, D.L.; Kendon, E.J.; Marsham, J.H.; Parker, D.J.; Stratton, R.A.; Tomassini, L.; Tucker, S. The effect of explicit convection on couplings between rainfall, humidity and ascent over Africa under climate change. *J. Clim.* **2020**, 1–60. [CrossRef]

40. Kendon, E.J.; Stratton, R.A.; Tucker, S.; Marsham, J.H.; Berthou, S.; Rowell, D.P.; Senior, C.A. Enhanced future changes in wet and dry extremes over Africa at convection-permitting scale. *Nat. Commun.* **2019**, *10*, 1–14. [CrossRef]

41. Weisman, M.L.; Klemp, J.B. The Dependence of Numerically Simulated Convective Storms on Vertical Wind Shear and Buoyancy. *Mon. Weather Rev.* **1982**, *110*, 504–520. [CrossRef]

42. Reynolds, R.W.; Smith, T.M.; Liu, C.; Chelton, D.B.; Casey, K.S.; Schlax, M.G. Daily High-Resolution-Blended Analyses for Sea Surface Temperature. *J. Clim.* **2007**, *20*, 5473–5496. [CrossRef]

43. Cook, K.H. Generation of the African Easterly Jet and Its Role in Determining West African Precipitation. *J. Clim.* **1999**, *12*, 1165–1184. [CrossRef]

44. Joyce, R.J.; Janowiak, J.E.; Arkin, P.A.; Xie, P. cMORPH: A method that produces global precipitation estimates from passive microwave and infrared data at high spatial and temporal resolution. *J. Hydrometeor.* **2004**, *5*, 487–503. [CrossRef]

45. Huffman, G.J.; Bolvin, D.T.; Nelkin, E.J.; Wolff, D.B.; Adler, R.F.; Gu, G.; Hong, Y.; Bowman, K.P.; Stocker, E.F. The TRMM Multisatellite Precipitation Analysis (TMPA): Quasi-Global, Multiyear, Combined-Sensor Precipitation Estimates at Fine Scales. *J. Hydrometeor.* **2007**, *8*, 38–55. [CrossRef]

46. Habib, E.; Haile, A.T.; Tian, Y.; Joyce, R.J. Evaluation of the High-Resolution CMORPH Satellite Rainfall Product Using Dense Rain Gauge Observations and Radar-Based Estimates. *J. Hydrometeor.* **2012**, *13*, 1784–1798. [CrossRef]

47. Dinku, T.; Ceccato, P.; Grover-Kopec, E.; Lemma, M.; Connor, S.J.; Ropelewski, C.F. Validation of satellite rainfall products over East Africa's complex topography. *Int. J. Remote Sens.* **2007**, *28*, 1503–1526. [CrossRef]

48. Romilly, T.G.; Gebremichael, M. Evaluation of satellite rainfall estimates over Ethiopian river basins. *Hydrol. Earth Syst. Sci.* **2011**, *15*, 1505–1514. [CrossRef]

49. Hirpa, F.A.; Gebremichael, M.; Hopson, T. Evaluation of High-Resolution Satellite Precipitation Products over Very Complex Terrain in Ethiopia. *J. Appl. Meteorol. Climatol.* **2010**, *49*, 1044–1051. [CrossRef]

50. Alfaro, D.A. Low-Tropospheric Shear in the Structure of Squall Lines: Impacts on Latent Heating under Layer-Lifting Ascent. *J. Atmos. Sci.* **2017**, *74*, 229–248. [CrossRef]

51. Dinku, T.; Connor, S.J.; Ceccato, P. Comparison of CMORPH and TRMM-3B42 over mountainous regions of Africa and South America. In *Satellite Rainfall Applications for Surface Hydrology*; Springer: Dordrecht, The Netherlands, 2010; pp. 193–204.

52. Stephens, G.L.; L'Ecuyer, T.; Forbes, R.; Gettelmen, A.; Golaz, J.-C.; Bodas-Salcedo, A.; Suzuki, K.; Gabriel, P.; Haynes, J. Dreary state of precipitation in global models. *J. Geophys. Res. Space Phys.* **2010**, *115*. [CrossRef]

53. Joseph, P.V.; Sijikumar, S. Intraseasonal Variability of the Low-Level Jet Stream of the Asian Summer Monsoon. *J. Clim.* **2004**, *17*, 1449–1458. [CrossRef]

54. Pithan, F.; Shepherd, T.G.; Zappa, G.; Sandu, I. Climate model biases in jet streams, blocking and storm tracks resulting from missing orographic drag. *Geophys. Res. Lett.* **2016**, *43*, 7231–7240. [CrossRef]

55. Prein, A.F.; Langhans, W.; Fosser, G.; Ferrone, A.; Ban, N.; Goergen, K.; Keller, M.; Toelle, M.; Gutjahr, O.; Feser, F.; et al. A review on regional convection-permitting climate modeling: Demonstrations, prospects, and challenges. *Rev. Geophys.* **2015**, *53*, 323–361. [CrossRef] [PubMed]

56. Parker, D.J.; Burton, R.R.; Diongue-Niang, A.; Ellis, R.J.; Felton, M.; Taylor, C.M.; Thorncroft, C.D.; Bessemoulin, P.; Tompkins, A.M. The diurnal cycle of the West African monsoon circulation. *Q. J. R. Meteorol. Soc.* **2005**, *131*, 2839–2860. [CrossRef]

57. Rotunno, R.; Klemp, J.B.; Weisman, M.L. A theory for strong, long-lived squall lines. *J. Atmos. Sci.* **1988**, *45*, 463–485. [CrossRef]

58. Van Vuuren, D.; Edmonds, J.; Kainuma, M.; Riahi, K.; Thomson, A.; Hibbard, K.; Hurtt, G.C.; Kram, T.; Krey, V.; Lamarque, J.-F.; et al. The representative concentration pathways: An overview. *Clim. Chang.* **2011**, *109*, 5–31. [CrossRef]

59. Prein, A.F.; Rasmussen, R.; Stephens, G. Challenges and Advances in Convection-Permitting Climate Modeling. *Bull. Am. Meteorol. Soc.* **2017**, *98*, 1027–1030. [CrossRef]

60. Hastings, D.A.; Paula, K.D.; Gerald, M.E.; Mark, B.; Hiroshi, M.; Hiroshi, M.; Hiroshi, M.; Peter, H.; John, P.; Nevin, A.B.; et al. *The Global Land One-Kilometer Base Elevation (GLOBE) Digital Elevation Model, Version 1.0.*; National Oceanic and Atmospheric Administration, National Geophysical Data Center: Boulder, CO, USA, 1999.